Perpendicularly Arranged Ruthenium Porphyrin Dimers and Trimers

Kenji Funatsu,[†] Akira Kimura,[†] Taira Imamura,*[,†] Akio Ichimura,[‡] and Yoichi Sasaki[†]

Division of Chemistry, Graduate School of Science, Hokkaido University, Sapporo 060, Japan, and Department of Chemistry, Faculty of Science, Osaka City University, Osaka 558, Japan

Received September 18, 1996[⊗]

A series of ruthenium(II) porphyrin dimers and trimers (carbonyl dimers, **1**−**4**; carbonyl trimers, **5**−**7**, bis(pyridyl) trimers, **8**−**10**), having axial or bridging porphyrin ligands, were synthesized and characterized by ^{1}H NMR and IR spectroscopy and mass spectrometry. An X-ray structural determination of $Ru^{II}(OEP)(CO)(H_2PyP_3P)$ (**1**) (OEP = octaethylporphyrinato dianion, H_2PyP_3P = 5-pyridyl-10,15,20-triphenylporphyrinato dianion) was carried out. The axial porphyrin ligand is coordinated to the ruthenium porphyrin subunit obliquely. The Ru−N(Py) bond length is 2.237(4) Å, and the angle between the ruthenium porphyrin macrocycle and the pyridyl ring is 63.23(35)°. Crystallographic data for **1** are as follows: chemical formula $C_{80}H_{73}N_9ORu\cdot CH_2Cl_2$, triclinic, $P\bar{1}$, a = 14.954(5) Å, b = 25.792(5) Å, c = 10.124(3) Å, α = 90.21(2)°, β = 108.43(2)°, γ = 73.39(2)°, Z = 2, $R(F)$ = 0.0674. ^{1}H NMR signals of 2,6- and 3,5-pyridyl protons of the axial ligand porphyrins of the oligomers **1**−**10** showed significant upfield shifts, indicating that the axial porphyrin subunits are coordinated to the ruthenium porphyrin subunits through the pyridyl group in solution. UV−vis spectra revealed the presence of excitonic interaction between two axial ligand porphyrin subunits in the trimers **8**−**10**. The MLCT bands from the central ruthenium(II) ions to the octaethylporphyrin rings were observed around 450 nm in **8** and **9**. Cyclic voltammograms of the carbonyl dimers and trimers showed no redox waves of the ruthenium(II) ions, because the ruthenium(II) oxidation state of these complexes was significantly stabilized by the coordination of the axial CO ligands. On the other hand, bis(pyridyl) trimers exhibit the Ru(III/II) waves in the region of −0.12 to +0.15 V vs Ag/Ag^+ reference electrode.

Introduction

Many flat- and gable-porphyrin oligomers linked by organic spacers have been synthesized as models for photosynthetic reaction centers to clarify effective factors such as inter-porphyrin distance and orientation as well as the number of porphyrin pigments on the photoinduced long-distance electron or energy transfer reaction processes.[1] Porphyrin oligomers having more than three porphyrin pigments have also been noted as synthetic molecular devices and models of light-harvesting systems.[2] The ruthenium dimer with a biphenylene organic spacer showed the unusual properties of taking a variety of small nitrogen molecules such as N_2 and N_2H_2 between the cofacially arranged porphyrin subunits and demonstrated the probability of molecular electrode catalysts for the reduction of N_2.[3] Similar cofacial cobalt(II) porphyrin dimers have also been examined as catalysts of electrochemical reduction of oxygen to water.[4] Thus, porphyrin oligomers have revealed fascinating photochemical and catalytic properties.

Sanders et al. achieved the construction of a cyclic zinc porphyrin trimer linked by 1,4-biphenylbutadiyne spacers, which catalyzed Diels−Alder reactions stereoselectively.[5] In the process of preparation, a new synthetic strategy using stereoselective template reactions was used; i.e., the zinc trimer was synthesized by a proper template reaction of tripyridyltriazine.[6]

Other approaches to construct porphyrin oligomers include a ligation method of *meso*-pyridylporphyrins, e.g., a stable

† Hokkaido University.
‡ Osaka City University.
⊗ Abstract published in *Advance ACS Abstracts*, March 1, 1997.

(1) (a) Sessler, J. L.; Johnson, M. R.; Lin, T. Y.; Creager, S. E. *J. Am. Chem. Soc.* **1988**, *110*, 3659. (b) Osuka, A.; Maruyama, K. *J. Am. Chem. Soc.* **1988**, *110*, 4454. (c) Harriman, A.; Odobel, F., Sauvage, J. P. *J. Am. Chem. Soc.* **1994**, *116*, 5481. (d) Wasielewski, M. R.; Johnson, D. G.; Niemczyk, M. P.; Gaines, G. L., III; O'Neil, M. P.; Svec, W. A. *J. Am. Chem. Soc.* **1990**, *112*, 6482. (e) Osuka, A.; Nakajima, S.; Maruyama, K. *J. Org. Chem.* **1992**, *57*, 7255. (f) Markl, G.; Reiss, M.; Keitmeier, P.; Noth, H. *Angew. Chem., Int. Ed. Engl.* **1995**, *34*, 2230. (g) Chang, C. K.; Abdalmuhdi, I. *J. Org. Chem.* **1983**, *48*, 5388. (h) Tabushi, I.; Sasaki, T. *Tetrahedron Lett.* **1982**, *23*, 1913. (i) Sessler, J. L.; Johnson, M. R.; Creager, S. E.; Fettinger, J. C.; Ibers, J. A. *J. Am. Chem. Soc.* **1990**, *112*, 9310. (j) Senge, O. M.; Gerzevske, K. R.; Vicente, M. G. H.; Forsyth, T. P.; Smith, K. M. *Angew. Chem., Int. Ed. Engl.* **1993**, *32*, 750. (k) Burrell, A. K.; Officer, D. L.; Reid, D. C. W. *Angew. Chem., Int. Ed. Engl.* **1995**, *34*, 900. (l) Chambron, J. C.; Heutz. V.; Sauvage, J. P. *Bull. Soc. Chim. Fr.* **1995**, *132*, 340. (m) Kurreck, H.; Huber, M. *Angew. Chem., Int. Ed. Engl.* **1995**, *34*, 849. (n) Autret, M.; Plouzennec, L. M.; Moinet, C.; Simonneaux, G. *J. Chem. Soc., Chem. Commun.* **1994**, 1169.

(2) (a) Harriman, J. D. A.; Milgram, L. R. *Chem. Phys. Lett.* **1987**, *136*, 427. (b) Anderson, H. L.; Hunter, C. A.; Sanders, J. K. M. *J. Chem. Soc., Chem. Commun.* **1989**, 226. (c) Anderson, S.; Anderson, H. L.; Bashall, A.; McPartlin, M.; Sanders, J. K. M. *Angew. Chem., Int. Ed. Engl.* **1995**, *34*, 1096. (d) Nagata, T.; Osuka, A.; Maruyama, K. *J. Am. Chem. Soc.* **1990**, *112*, 3054. (e) Osuka, A.; Liu, B. L.; Maruyama, K. *Chem. Lett.* **1993**, 949. (f) Osuka, A.; Tanabe, N.; Zhang, R. P.; Maruyama, K. *Chem. Lett.* **1993**, 1505. (g) Prathapan, S.; Johnson, T. E.; Linsey, J. S. *J. Am. Chem. Soc.* **1993**, *115*, 7519. (h) Wanger, R. W.; Linsey, J. S. *J. Am. Chem. Soc.* **1994**, *116*, 9759. (i) Seth, J.; Palaniappan, V.; Johnson, T. E.; Prathapan, S.; Linsey, J. S.; Bocian, D. F. *J. Am. Chem. Soc.* **1995**, *116*, 10578. (j) Segawa, H.; Kunimoto, K.; Susumu, K.; Taniguchi, M.; Shimidzu, T. *J. Am. Chem. Soc.* **1994**, *116*, 11193. (k) Susumu, K.; Kunimoto, K.; Segawa, H.; Shimidzu, T. *J. Phys. Chem.* **1995**, *99*, 29. (l) Drain, C. M.; Lehn, J. M. *J. Chem. Soc., Chem. Commun.* **1994**, 2313. (m) Bonnet, R.; Ioannou, S.; Pearson, C.; Petty, M. C.; Evans, M. R.; Willkins, R. F. *J. Mater. Chem.* **1995**, *5*, 237.

(3) (a) Collman, J. P.; Huchison, J. E.; Lopez, M. A.; Guilard, R. *J. Am. Chem. Soc.* **1992**, *114*, 8066. (b) Collman, J. P.; Hutchison, J. E.; Ennis, M. S.; Lopez, M. a.; Guilard, R. *J. Am. Chem. Soc*. **1992**, *114*, 8074.

(4) (a) Collman, J. P.; Denisevich, P.; Konai, Y.; Marrocco, M.; Koval, C.; Anson, F. C. *J. Am. Chem. Soc.* **1980**, *102*, 6027. (b) Durand, R. R., Jr.; Bencosme, C. S.; Collman, J. P.; Anson, F. C. *J. Am. Chem. Soc.* **1983**, *105*, 2710. (c) Chang, C. K.; Liu, H. Y.; Abdalmuhdi, I. *J. Am. Chem. Soc.* **1984**, *106*, 2725. (d) Mest, Y. L.; L'Her, M. *J. Chem. Soc., Chem. Commun.* **1995**, 1441. (e) Guilard, R.; Brandes, S.; Tardieux, C.; Tabard, A.; L'Her, M.; Miry, C.; Gouerec, P.; Knop, Y.; Collman, J. P. *J. Am. Chem. Soc.* **1995**, *117*, 11721.

(5) (a) Lindoy, L. F. *Nature* **1994**, 368, 96. (b) Bonar-Law, R. P.; Mackay, L. G.; Walter, C. J.; Marvaud, V.; Sanders, J. K. M. *Pure Appl. Chem.* **1994**, *66*, 803.

(6) (a) Anderson, H.; Anderson, H. L.; Sanders, J. K. M. *Acc. Chem. Res.* **1993**, *26*, 469. (b) McCallien, D. W. J.; Sanders, J. K. M. *J. Am. Chem. Soc.* **1995**, *117*, 6611.

S0020-1669(96)01154-8 CCC: $14.00

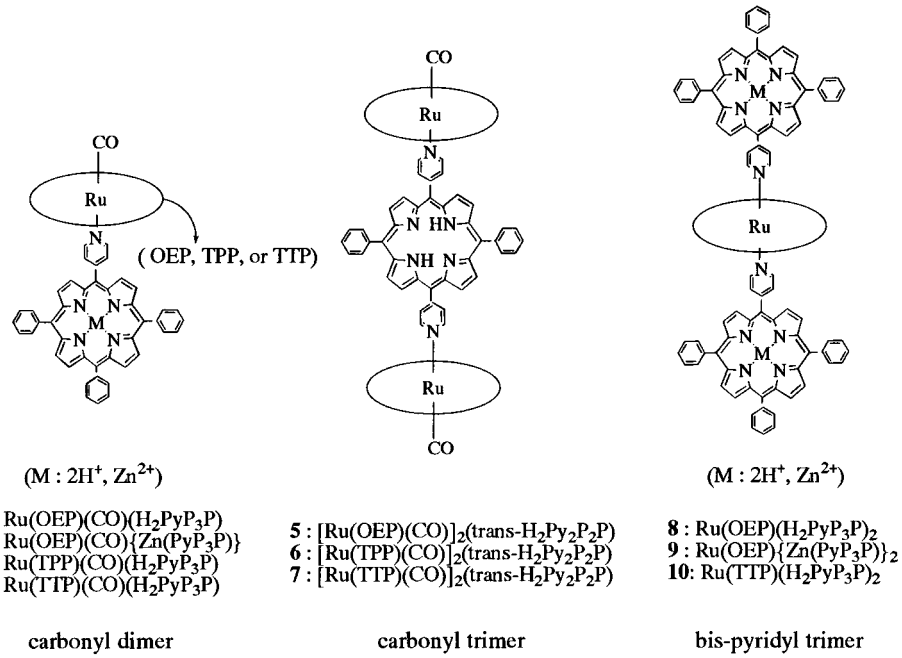

Figure 1. Ruthenium porphyrin oligomers.

porphyrin dimer and tetramer were synthesized by the ligation of mono(pyridyl)porphyrins or that of zinc complexes to square planer Pt(II) and Pd(II) arrays.[7] Fleischer and Shachater also reported some oligomers as a result of the treatment of *meso*-pyridylporphyrins with zinc tetraphenylporphyrin complexes.[8] The X-ray crystal structural determination for a tetramer clarified that the pyridyl substituents were bound to the zinc ions with an unusual tilt. ^{1}H NMR mesurements indicated that Zn(TPP)-(H_2PyP_3P), [Zn(TPP)]$_2$(*cis*-$H_2Py_2P_2P$), and [Zn(TPP)]$_2$(*trans*-$H_2Py_2P_2P$) were present in solution.[8,9] A novel cyclic ruthenium porphyrin tetramer [Ru(PyP_3P)(CO)]$_4$ was also synthesized.[10] The ruthenium tetramer was successfully isolated, because of the stability of the Ru−N(Py) bond unlike the zinc porphyrin oligomers. Furthermore, a ruthenium porphyrin pentamer [Ru(TPP)(CO)]$_4${Zn(Py_4P)} was recently prepared by the ligation of four pyridyl substituents of tetrapyridylporphyrin to four ruthenium tetraarylporphyrin monomers.[11] A series of similar osmium(II) porphyrin oligomers, Os(OEP)(CO)(H_2PyP_3P), [Os(OEP)(CO)]$_2$(*trans*-$H_2Py_2P_2P$), [Os(OEP)(CO)]$_2$(*cis*-$H_2Py_2P_2P$), [Os(OEP)(CO)]$_3$(H_2Py_3PP), and [Os(OEP)(CO)]$_4$(H_2Py_4P), were also independently prepared and characterized.[12] These zinc, ruthenium, and osmium porphyrin oligomers have a characteristic perpendicular geometry between zinc, ruthenium, or osmium porphyrin subunits and axial porphyrin subunits. In addition, there are a few reports outlining the synthesis and photophysical properties of "axial-bonding type" phosphorus(V) porphyrin dimers and trimers[13] and of a porphyrin and sapphyrin pair bound electrostatically.[14] Thus, perpendicularly linking porphyrin oligomers have recently gained a lot of attention, because the synthesis, structure, properties, and probabilities as a functional molecule are of great interest.

Herein, we report the synthesis and characterization of a series of perpendicularly linking ruthenium porphyrin oligomers (**1**−**4**, carbonyl dimers; **5**−**7**, carbonyl trimers; **8**−**10**, bis(pyridyl) trimers) (Figure 1). The X-ray crystal structure of **1** is also reported. The structure of the oligomers in solution was discussed on the basis of NMR ring current shifts of pyridyl protons in comparison with those of corresponding monomers Ru(OEP)(CO)(Py), Ru(TPP)(CO)(Py), and Ru(OEP)(Py)$_2$. Interactions between porphyrin subunits in a molecule were also discussed on UV−vis spectroscopic and electrochemical properties of the oligomers **1**−**10**, in which **1**, **2**, **5**, and **8** were previously reported in a preliminary account (Figure 1).[15]

Experimental Section

Materials. H_2TPP was obtained as a byproduct of *meso*-pyridylporphyrin ligands described below. H_2OEP and H_2TTP were prepared according to the methods described in the literature.[16] Triruthenium(0) dodecacarbonyl, $Ru_3(CO)_{12}$, was purchased from Aldrich. Silica gel (Wakogel C-300, 200) and alumina (Wolem, neutral, activity II) were used for column chromatography. Ru^{II}(TPP)(CO)(MeOH) and Ru^{II}(OEP)(CO)(MeOH) were prepared as described in the literature.[17] Ru^{II}(TTP)(CO)(MeOH) was prepared by a method analogous to that used for Ru^{II}(TPP)(CO)(MeOH). ^{1}H NMR, UV−vis, and IR spectroscopic data for these complexes agreed well with the reported values, and the elemental analyses were also satisfactory.[17] These data are given below for comparison to the new oligomers as follows.

Ru^{II}(OEP)(CO)(MeOH). Anal. Calcd for $C_{38}H_{48}N_4O_2Ru$: C, 65.77; H, 6.97; N, 8.08. Found: C, 66.00; H, 7.01; N, 7.93. UV−vis (CH_2Cl_2): λ_{max}/nm 392 (Soret), 517, 548. IR (KBr): ν_{CO} 1950, 1923

(7) Yuan, H.; Thomas, L.; Woo, K. *Inorg. Chem.* **1996**, *35*, 2808.
(8) Fleischer, E. B.; Shachter, A. M. *Inorg. Chem.* **1991**, *30*, 3763.
(9) Abbreviations: TPP = 5,10,15,20-tetraphenylporphyrinato dianion; OEP = 2,3,7,8,12,13,17,18-octaethylporphyrinato dianion; TTP = 5,10,15,20-tetratolylporphyrinato dianion; H_2PyP_3P = 5-pyridyl-10,15,20-triphenylporphyrin; *cis*-$H_2Py_2P_2P$ = 5,10-dipyridyl-15,20-diphenylporphyrin; *trans*-$H_2Py_2P_2P$ = 5,15-dipyridyl-10,20-diphenylporphyrin; H_2Py_3PP = 5,10,15-tripyridyl-20-phenylporphyrin; H_2Py_4P = 5,10,15,20-tetrapyridylporphyrin; Py = pyridine; (TBA)-PF_6 = *n*-tetrabutylammonium hexafluorophosphate; Por = porphyrinato dianion unspecified.
(10) Funatsu, K.; Kimura, A.; Imamura, T.; Sasaki, Y. *Chem. Lett.* **1996**, 765.
(11) Alessio, E.; Macchi, M.; Heath, S.; Marzill, L. G. *J. Chem. Soc., Chem. Commun.* **1996**, 1411.
(12) Kariya, N.; Imamura, T.; Sasaki, Y. *Inorg. Chem.* **1997**, *36*, 833.
(13) (a) Susumu, K.; Segawa, H.; Shimidzu, T. *Chem. Lett.* **1995**, 929. (b) Rao, T. A.; Maiya, B. G. *J. Chem. Soc., Chem. Commun.* **1995**, 939.
(14) Kral, V.; Springs, S. L.; Sessler, J. L. *J. Am. Chem. Soc.* **1995**, *117*, 8881.
(15) Kimura, A.; Funatsu, K.; Imamura, T.; Kido, H.; Sasaki, Y. *Chem. Lett.* **1995**, 207.
(16) Paine, J. P., III; Kirshner, W. B.; Moskowitz, D. W. *J. Org. Chem.* **1976**, *41*, 3857.
(17) Collman, J. P.; Barnes, C. E.; Brothers, P. J.; Collins, T. J.; Ozawa, T.; Gallucci, J. C.; Ibers, J. A. *J. Am. Chem. Soc.* **1984**, *106*, 5151.

cm^{-1}. ^{1}H NMR (CD_2Cl_2, 270 MHz) (δ/ppm): H_{meso} 9.95 (s); CH_3***CH*****$_2$** 4.11 (q, 7.56 Hz); ***CH*****$_3$**CH_2 1.94 (t, 7.56 Hz).

Ru^{II}(TPP)(CO)(MeOH). Anal. Calcd for $C_{46}H_{32}N_4O_2Ru$: C, 71.34; H, 4.17; N, 7.24. Found: C, 71.42; H, 4.36; N, 7.11. UV−vis (CH_2Cl_2): λ_{max}/nm 413 (Soret), 532, 569 (sh). IR (KBr): ν_{CO} 1944 cm^{-1}. ^{1}H NMR (CD_2Cl_2, 270 MHz) (δ/ppm): H_β 8.67 (s); H_o 8.25 (d), 8.07 (d); $H_{m,p}$ 7.69 (m).

Ru^{II}(TTP)(CO)(MeOH). Anal. Calcd for $C_{50}H_{40}N_4O_2Ru$: C, 72.35; H, 4.86; N, 6.75. Found: C, 71.96; H, 4.70; N, 6.88. UV−vis (CH_2Cl_2): λ_{max}/nm 417 (Soret), 530, 569 (sh). IR (KBr): ν_{CO} 1945 cm^{-1}. ^{1}H NMR (CD_2Cl_2, 270 MHz) (δ/ppm): H_β 8.69 (s); H_o 8.07 (d), 7.99 (d); $H_{m,p}$ 7.53 (m); H−CH_3 2.66 (s).

Synthesis of Axial Porphyrin Ligands. Porphyrins containing pyridyl groups, H_2PyP_3P and *trans*-$H_2Py_2P_2P$, were synthesized according to the literature and separated using silica gel columns.[8,18] When benzaldehyde (15 mL), isonicotinaldehyde (5 mL), and pyrrole (14 mL) were used for the preparation of these porphyrin ligands, the amounts of H_2PyP_3P and *trans*-$H_2Py_2P_2P$ were 1.44 g and 27.5 mg, respectively, which correspond to 29 and 0.56% yields of the total amount of the products obtained by chromatography. The porphyrins purified were identified by thin-layer chromatography, elemental analysis, visible spectroscopy, and ^{1}H NMR measurements. These data agreed well with the reported results.[8] ^{1}H NMR for H_2PyP_3P (CD_2Cl_2, 400 MHz): H_{NH} −2.88 (s, 2H), H_β 8.85 (m, 8H), H_o 8.20 (m, 6H), $H_{m,p}$ 7.77 (m, 9H), $H_{2,6\text{-Py}}$ 8.98 (dd, 2H), $H_{3,5\text{-Py}}$ 8.15 (dd, 2H) ppm. ^{1}H NMR for *trans*-$H_2Py_2P_2P$: H_{NH} −2.92 (s, 2H), H_β 8.87 (m, 8H), H_o 8.19 (m, 4H), $H_{m,p}$ 7.77 (m, 6H), $H_{2,6\text{-Py}}$ 8.99 (dd, 4H), $H_{3,5\text{-Py}}$ 8.15 (dd, 4H) ppm.

Zn(PyP$_3$P). The zinc porphyrin, Zn(PyP_3P), was prepared according to the method described in the literature.[8] A mixed solution of toluene (40 mL) and 2,6-lutidine (10 mL) was added to the acetone solution (40 mL) containing $ZnCl_2$ (270 mg). To the solution, H_2PyP_3P (200 mg) was added and stirred for 4 h at room temperature until the absorption around 650 nm from the free ligand had disappeared. After the addition of distilled water (100 mL), the solution was left to stand for several hours. The organic layer was concentrated by evaporation and diluted with ethanol (150 mL) and left to stand for 1 night. The solid product thus obtained was filtered out and dissolved in dichloromethane. The solution was loaded on a silica gel column followed by elution with dichloromethane. The crude product obtained by evaporation was recrystallized using toluene−hexane. The absorption spectrum of the complex having bands at 424, 554, and 594 nm was similar to the reported one.[8]

Ru^{II}(OEP)(CO)(H$_2$PyP$_3$P) (1). Ru^{II}(OEP)(CO)(MeOH) (48 mg, 6.9 × 10^{-5} mol) and H_2PyP_3P (48 mg, 7.8 × 10^{-5} mol) were dissolved in a spectral grade of toluene which was bubbled with argon before use. The solution was refluxed for 30 min under argon, cooled to room temperature, and evaporated to dryness. The solid material was dissolved in a small amount of dichloromethane which was purified immediately before use. The solution was loaded on a silica gel column and eluted with dichloromethane. The first red fraction was collected and dried to give a product. The red product was recrystallized from toluene−hexane and dried at 110 °C in vacuo for 5 h (yield: 60 mg, 67.5%). Planar single crystals suitable for X-ray crystallography were obtained from dichloromethane−methanol.

Anal. Calcd for $C_{80}H_{73}N_9ORu$: C, 75.21; H, 5.76; N, 9.87. Found: C, 75.37; H, 5.92; N, 10.00. ^{1}H NMR (CD_2Cl_2, 270 MHz): H_{meso} 10.01 (s, 4H); CH_3***CH*****$_2$** 4.08 (q, 8H); ***CH*****$_3$**CH_2 1.96 (t, 12H); H_o 8.04 (m, 2H), 7.95 (m, 4H); $H_{m,p}$ 7.68 (m, 9H); H_β 8.69 (d, 2H), 8.65 (d, 2H), 8.36 (d, 2H), 7.16 (d, 2H); $H_{3,5\text{-Py}}$ 5.77 (d, 2H); $H_{2,6\text{-Py}}$ 1.23 (d, 2H); H_{NH} −3.41 (s, 2H) ppm. UV−vis (CH_2Cl_2) (log ϵ): λ_{max}/nm 395 (5.48), 418 (5.60), 514 (4.50), 550 (4.47), 590 (3.73), 646 (3.60). IR (KBr): ν_{CO} 1945 cm^{-1}. FAB-MS (matrix: 3-nitrobenzyl alcohol = NBA) shows a sharp parent peak at 1277 (m/z^+).

Ru^{II}(OEP)(CO){Zn(PyP$_3$P)} (2). Ru^{II}(OEP)(CO){Zn(PyP_3P)} was synthesized by a method similar to that of Ru^{II}(OEP)(CO)(H_2PyP_3P) using Zn(PyP_3P) in place of H_2PyP_3P. Ru^{II}(OEP)(CO)(MeOH) (20 mg, 2.9 × 10^{-5} mol) and Zn(PyP_3P) (20 mg, 2.9 × 10^{-5} mol) were dissolved in a spectral grade of toluene which was bubbled with argon before use. The solution was refluxed for 1 h under argon atmosphere, cooled to room temperature, and evaporated to dryness. The reddish-purple solid was dissolved in a small amount of dichloromethane purified immediately before use. The solution was loaded on a silica gel column and eluted with dichloromethane as an eluent. A red eluate was dried to give a product. The product was recrystallized from toluene−hexane and dried at 100 °C in vacuo for 5 h (yield: 34 mg, 88.3%).

Anal. Calcd for $C_{80}H_{71}N_9ORuZn$: C, 71.65; H, 5.34; N, 9.40. Found: C, 71.62; H, 5.32; N, 9.37. ^{1}H NMR (CD_2Cl_2, 270 MHz): H_{meso} 10.04 (s, 4H); CH_3***CH*****$_2$** 4.09 (q, 8H); ***CH*****$_3$**CH_2 2.02 (t, 12H); H_o 7.97 (m, 2H), 7.85 (m, 4H); $H_{m,p}$ 7.45 (m, 9H); H_β 8.76 (d, 2H), 8.72 (d, 2H), 8.45 (d, 2H), 7.24 (d, 2H); $H_{3,5\text{-Py}}$ 5.79 (d, 2H); $H_{2,6\text{-Py}}$ 1.26 (d, 2H) ppm. UV−vis (CH_2Cl_2) (log ϵ): λ_{max}/nm 395 (5.45), 419 (5.71), 516 (4.18), 548 (4.63), 586 (3.64). IR (KBr): ν_{CO} 1941 cm^{-1}. FAB-MS (NBA) shows a sharp parent peak at 1340 (m/z^+).

Ru^{II}(TPP)(CO)(H$_2$PyP$_3$P) (3). Ru(TPP)(CO)(EtOH) (50 mg, 6.3 × 10^{-5} mol) and H_2PyP_3P (50 mg, 8.1 × 10^{-5} mol) were dissolved in 2-methoxyethanol ($CH_3OCH_2CH_2OH$) (70 mL), which was bubbled with argon for 20 min before use. The solution was refluxed for 1 h, cooled to room temperature, and filtered through a sintered glass before addition of water (50 mL). A red colored precipitate thus obtained was filtered off, washed with water, dissolved in CH_2Cl_2, and finally purified by column chromatography using a silica gel column. The first red eluate was dried up. The solid material was recrystallized from dichloromethane−methanol. The reddish-purple product was dried at 100 °C in vacuo for 3 h (yield: 78 mg, 71%).

Anal. Calcd as $C_{88}H_{57}N_9ORu$: C, 77.85; H, 4.23; N, 9.29. Found: C, 77.85; H, 4.84; N, 9.16. ^{1}H NMR (CD_2Cl_2, 270 MHz): H*o* 8.32 (m, 4H), 8.19 (m, 4H), 8.08 (m, 2H), 8.00 (m, 4H); $H_{m,p}$ 7.7−7.5 (m, 21H); H_β 8.75 (10H), 8.70 (d, 2H), 8.46 (d, 2H), 7.30 (d, 2H); $H_{3,5\text{-Py}}$ 6.10 (d, 2H); $H_{2,6\text{-Py}}$ 1.92 (d, 2H); H_{NH} −3.33 (s, 2H) ppm. UV−vis (CH_2Cl_2) (log ϵ): λ_{max}/nm 419 (5.84), 519 (4.44), 530 (sh), 550 (sh), 588 (3.79), 645 (3.60). IR (KBr): ν_{CO} 1968, 1953 cm^{-1}. FAB-MS (NBA) shows a sharp parent peak at 1358 (m/z^+).

Ru^{II}(TTP)(CO)(H$_2$PyP$_3$P) (4). Ru^{II}(TTP)(CO)(H_2PyP_3P) was synthesized by a method similar to that of Ru^{II}(OEP)(CO)(H_2PyP_3P) using Ru^{II}(TTP)(CO)(MeOH) instead of Ru^{II}(OEP)(CO)(MeOH). Ru^{II}(TTP)(CO)(MeOH) (100 mg, 1.2 × 10^{-4} mol) and H_2PyP_3P (75 mg, 1.2 × 10^{-4} mol) were dissolved in a spectral grade of toluene which was bubbled with argon before use. The solution was refluxed for 1 h under argon, cooled to room temperature, and evaporated to dryness. The solid material was dissolved in a small amount of dichloromethane. The solution was loaded on a silica gel column and eluted with dichloromethane. A red eluate was evaporated to dryness. The product was recrystallized from dichloromethane−methanol. The red product was dried at 110 °C in vacuo for 3 h (yield: 130 mg, 77%).

Anal. Calcd for $C_{92}H_{65}N_9ORu$: C, 78.16; H, 4.63; N, 8.92. Found: C, 78.73; H, 4.98: N, 9.03. ^{1}H NMR (CD_2Cl_2, 270 MHz): H_o 8.19 (m, 4H), 8.07 (m, 6H), 8.01 (m, 4H); $H_{m,p}$ 7.7−7.5 (m, 17H); H_β 8.75 (10H), 8.72 (d, 2H), 8.46 (d, 2H), 7.30 (d, 2H); H−CH_3 2.67 (s, 12H); $H_{3,5\text{-Py}}$ 6.06 (d, 2H); $H_{2,6\text{-Py}}$ 1.91 (d, 2H); H_{NH} −3.32 (s, 2H) ppm. UV−vis (CH_2Cl_2) (log ϵ): λ_{max}/nm 417 (5.86), 519 (4.45), 530 (sh), 550 (sh), 589 (3.85), 647 (3.73). IR (KBr): ν_{CO} 1952 cm^{-1}. FAB-MS (NBA) shows a sharp parent peak at 1413 (m/z^+).

[Ru^{II}(OEP)(CO)]$_2$(*trans*-H$_2$Py$_2$P$_2$P) (5). Ru^{II}(OEP)(CO)(MeOH) (40 mg, 5.8 × 10^{-5} mol) and *trans*-$H_2Py_2P_2P$ (18 mg, 2.9 × 10^{-5} mol) were dissolved in toluene which was bubbled with argon before use. The solution was refluxed for 5 h with mixing and cooled to room temperature followed by evaporation to dryness. The resulting solid was dissolved in a small amount of toluene and chromatographed using an alumina column. A red band was collected using toluene as an eluent and evaporated to dryness (yield: 25 mg, 45%).

Anal. Calcd for $C_{116}H_{116}N_{14}O_2Ru_2$: C, 71.80; H, 6.03; N, 10.01. Found: C, 72.05; H, 6.19; N, 10.12. ^{1}H NMR (CD_2Cl_2, 270 MHz): H_{meso} 9.97 (s, 8H); CH_3***CH*****$_2$** 4.03 (q, 16H); ***CH*****$_3$**CH_2 1.90 (t, 24H); H*o* 7.7 (m, 4H); $H_{m,p}$ 7.7−7.5 (m, 6H); H_β 8.19 (d, 4H), 7.01 (d, 4H); $H_{3,5\text{-Py}}$ 5.62 (d, 4H); $H_{2,6\text{-Py}}$ 1.15 (d, 4H); H_{NH} −3.98 (s, 2H) ppm. UV−vis (CH_2Cl_2) (log ϵ): λ_{max}/nm 395 (5.71), 421 (5.59), 515 (4.67), 550 (4.80), 591 (3.72), 648 (3.57). IR (KBr): ν_{CO} 1942 cm^{-1}.

[Ru^{II}(TPP)(CO)]$_2$(*trans*-H$_2$Py$_2$P$_2$P) (6). Ru^{II}(TPP)(CO)(MeOH) (130 mg, 1.6 × 10^{-4} mol) and *trans*-$H_2Py_2P_2P$ (50 mg, 8.1 × 10^{-5} mol) were dissolved in toluene which was bubbled with argon before

(18) Alder, A. D.; Longo, F. R.; Finarelli, J. D.; Goldmacher, J.; Assour, J.; Korsalioff, L. *J. Org. Chem.* **1967**, *32*, 476.

use. The solution was refluxed for 2 h under argon, cooled to room temperature, and evaporated to dryness. The solid material was dissolved in a small amount of dichloromethane. The solution was loaded on a silica gel column and eluted with dichloromethane. A red eluate was evaporated to dryness. The product was recrystallized from dichloromethane−methanol and dried at 80 °C in vacuo for 3 h (yield: 30 mg, 17%).

Anal. Calcd for $C_{132}H_{84}N_{14}O_2Ru_2$: C, 75.48; H, 4.03; N, 9.34. Found: C, 75.56; H, 4.26; N, 9.20. ^{1}H NMR (CD_2Cl_2, 270 MHz): H_o 8.30−8.00 (m, 20H); $H_{m,p}$ 7.7−7.4 (m, 30H); H_β 8.69 (s, 16H), 8.20 (d, 4H), 7.19 (d, 4H); $H_{3,5\text{-Py}}$ 5.95 (d, 4H); $H_{2,6\text{-Py}}$ 1.85 (d, 4H); H_{NH} −3.80 (s, 2H) ppm. UV−vis (CH_2Cl_2) (log ϵ): λ_{max}/nm 414 (5.95), 520 (sh), 530 (4.65), 565 (sh), 589 (3.91), 646 (3.67). IR (KBr): ν_{CO} 1974, 1952 cm^{-1}.

[Ru^{II}(TTP)(CO)]$_2$(*trans*-H$_2$Py$_2$P$_2$P) (7). [Ru^{II}(TTP)(CO)]$_2$(*trans*-$H_2Py_2P_2P$) was synthesized by a method similar to [Ru^{II}(OEP)(CO)]$_2$(*trans*-$H_2Py_2P_2P$) using Ru^{II}(TTP)(CO)(MeOH). Ru^{II}(TTP)(CO)(MeOH) (55 mg, 6.6×10^{-5} mol) and *trans*-$H_2Py_2P_2P$ (20 mg, 3.3×10^{-5} mol) were dissolved in toluene which was bubbled with argon before use. The solution was refluxed for 2 h under argon, cooled to room temperature, and evaporated to dryness. The solid material was dissolved in a small amount of dichloromethane. The solution was loaded on a silica gel column and eluted with dichloromethane. A red eluate was evaporated to dryness. The red product was recrystallized from dichloromethane−hexane and dried at 110 °C in vacuo for 3h (yield: 41 mg, 55%).

Anal. Calcd for $C_{140}H_{100}N_{14}O_2Ru_2$: C, 76.00; H, 4.56; N, 8.87. Found: C, 75.70; H, 4.71; N, 8.86. ^{1}H NMR (CD_2Cl_2, 270 MHz): H_o 8.29 (m, 8H), 8.15 (m, 8H), 7.99 (m, 4H); $H_{m,p}$ 7.8−7.5 (m, 22H); H_β 8.71 (s, 16H), 8.14 (d, 4H), 7.17 (d, 4H); $H_{3,5\text{-Py}}$ 5.93 (d, 4H); $H_{2,6\text{-Py}}$ 1.83 (d, 4H); H_{NH} −3.82 (s, 2H) ppm. UV−vis (CH_2Cl_2) (log ϵ): λ_{max}/nm 414 (5.96), 520 (sh), 532 (4.66), 565 (sh), 586 (3.91), 646 (3.67). IR (KBr): ν_{CO} 1958 cm^{-1}.

Ru(OEP)(H$_2$PyP$_3$P)$_2$ (8). Dry toluene solution (700 mL) containing Ru(OEP)(CO)(MeOH) (60 mg, 8.6×10^{-5} mol) and H_2PyP_3P (106 mg, 1.7×10^{-4} mol) was photoirradiated with a 100 W medium-pressure mercury-vapor lamp for 8 h during vigorous stirring with Ar bubbling. The solution was concentrated to load on an alumina column. A brown fraction eluted with toluene was collected. The eluate was evaporated to dryness. The deep-purple solid was recrystallized from toluene−hexane and dried at 110 °C in vacuo for 3 h (yield: 100 mg, 63%).

Anal. Calcd as $C_{122}H_{102}N_{14}Ru$: C, 78.56; H, 5.51; N, 10.52. Found: C, 77.37; H, 5.60; N, 10.33. ^{1}H NMR (C_6D_6, 270 MHz): H_{meso} 10.06 (s, 4H); CH_3CH_2 4.09 (q, 8H); CH_3CH_2 2.08 (t, 12H); H_o 8.01 (m, 8H), 7.91 (m, 4H); $H_{m,p}$ −7.5 (m, 18H); H_β 8.79 (d, 4H), 8.77 (d, 4H), 8.25 (d, 4H), 6.93 (d, 4H); $H_{3,5\text{-Py}}$ 5.31 (d, 4H); $H_{2,6\text{-Py}}$ 2.82 (d, 4H); H_{NH} −2.81 (s, 4H) ppm. UV−vis ($C_6H_5CH_3$) (log ϵ): λ_{max}/nm 399 (sh), 419 (5.73), 456 (4.70), 516 (4.80), 546 (2.73), 588 (1.33), 652 (1.09), 650−750 (broad band). FAB-MS (NBA) shows a sharp parent peak at 1865 (m/z^+).

Ru(OEP){Zn(PyP$_3$P)}$_2$ (9). Ru^{II}(OEP)(H_2PyP_3P)$_2$ (50 mg, 2.7×10^{-5} mol) and $Zn(CH_3COO)_2$ (50 mg, 2.7×10^{-4} mol) were dissolved in a mixed solvent of toluene (35 mL) and ethanol (15 mL). The solution was vigorously stirred for 5 h at room temperature until the absorption around 650 nm due to the axial porphyrin of H_2PyP_3P had completely disappeared. The solution was evaporated to dryness. The solid material was dissolved in a small amount of toluene. The solution was loaded on an alumina column and eluted with toluene. A brown eluate was collected and evaporated to dryness. The product was recrystallized from toluene−hexane. The deep-purple product was dried at 110 °C in vacuo for 3 h (yield: 20 mg, 40%).

Anal. Calcd for $C_{122}H_{98}N_{14}RuZn_2$: C, 73.55; H, 4.23; N, 9.29. Found: C, 73.38; H, 5.04; N, 9.66. ^{1}H NMR (C_6D_6, 270 MHz): H_{meso} 10.10 (s, 4H); CH_3CH_2 4.11 (q, 8H); CH_3CH_2 2.07 (t, 12H); H_o ∼8.11 (m, 12H); $H_{m,p}$ ∼7.5 (m, 18H); H_β 8.96 (d, 4H), 8.92 (d, 4H), 8.40 (d, 4H), 7.11 (d, 4H); $H_{3,5\text{-Py}}$ 5.54 (d, 4H); $H_{2,6\text{-Py}}$ 2.96 (d, 4H) ppm. UV−vis ($C_6H_5CH_3$) (log ϵ): λ_{max}/nm 395 (5.23), 423 (5.82), 450 (sh), 523 (4.61), 547 (4.66), 594 (3.96), 653 (3.95). FAB-MS (NBA) shows a sharp parent peak at 1913 (m/z^+).

Ru(TTP)(H$_2$PyP$_3$P)$_2$ (10). Ru^{II}(TTP)(H_2PyP_3P)$_2$ was synthesized by a method similar to that for Ru^{II}(OEP)(H_2PyP_3P)$_2$ (**8**). A spectral grade toluene solution (700 mL) containing Ru(TTP)(CO)(MeOH) (60 mg, 7.2×10^{-5} mol) and H_2PyP_3P (90 mg, 1.4×10^{-4} mol) was photoirradiated with a 100 W medium-pressure mercury-vapor lamp for 6 h during vigorous stirring under Ar. The solution was concentrated to load on an alumina column. A brown band eluted with toluene was collected. The eluate was evaporated to dryness. The deep-purple solid material was recrystallized from toluene−hexane and dried at 110 °C in vacuo for 3 h (yield: 52 mg, 36%).

Anal. Calcd for $C_{134}H_{94}N_{14}Ru$: C, 80.41; H, 4.73; N, 9.81. Found: C, 71.55; H, 4.64; N, 9.69. ^{1}H NMR (C_6D_6, 270 MHz): H*o* 8.48 (m, 8H), 8.06 (m, 4H), 7.95 (m, 8H); $H_{m,p}$ ∼7.5 (m, 18H); H_β 9.01 (s, 8H), 8.84 (d, 4H), 8.82 (d, 4H), 8.55 (d, 4H), 7.55 (d, 4H); $H_{3,5\text{-Py}}$ 5.61 (d, 4H); $H_{2,6\text{-Py}}$ 3.49 (d, 4H); H−CH_3 2.46 (s, 12H) ppm. UV−vis ($C_6H_5CH_3$) (log ϵ): λ_{max}/nm 418 (5.83), 511 (4.77), 547 (4.26), 592 (4.17), 652 (4.13), 650−750 (broad band).

Table 1. Crystallographic Data for **1**

formula	$C_{80}H_{73}N_9ORu\cdot CH_2Cl_2$
cryst syst	triclinic
space group	*P*1
a/Å	14.954(5)
b/Å	25.793(5)
c/Å	10.125(3)
α/deg	90.12(2)
β/deg	108.43(2)
γ/deg	73.39(2)
V/Å^3	3534.0(2)
Z	2
d_{calcd}/g cm^{-3}	1.282
cryst size/mm	0.50 × 0.70 × 0.30
scan mode	$\omega-2\theta$
scan speed/deg min^{-1}	6
$2\theta_{max}$/deg	55
h,*k*,*l* range	±20,±34,+14
no. of unique reflns	17 766
no. of obsd reflns	9316, $F_o > 6\sigma(F_o)$
R^a	0.0674
$R_w{}^a$	0.0816

^{a} $R = \sum||F_o| - |F_c||/\sum|F_o|$. ^{b} $R_w = (\sum w(|F_o| - |F_c|)^2/\sum w|F_o|^2)^{1/2}$.

Table 2. Selected Bond Distances of **1** (Å)^a

Ru−N1	2.050(4)	$C_\alpha-C_\beta$ (av for OEP)	1.459(9)
Ru−N2	2.042(5)	$C_\beta-C_\beta$ (av for OEP)	1.363(10)
Ru−N3	2.046(4)	$C_\alpha-C_m$ (av for OEP)	1.390(9)
Ru−N4	2.066(5)	N−C_α (av for H_2PyP_3P)	1.377(8)
Ru−N(Py)	2.237(4)	$C_\alpha-C_\beta$ (av for H_2PyP_3P)	1.451(9)
Ru−C(CO)	1.801(6)	$C_\beta-C_\beta$ (av for H_2PyP_3P)	1.378(9)
C(CO)−O(CO)	1.165(7)	$C_\alpha-C_m$ (av for H_2PyP_3P)	1.394(8)
N−C_α (av for OEP)	1.375(8)		

^{a} C_α, α-pyrrole carbon; C_β, *β*-pyrrole carbon; C_m, methine carbon.

X-ray Structural Determinations. X-ray data for **1** were collected with graphite-monochromated Mo Kα radiation on a Rigaku AFC-5R diffractometer at 23 °C. Unit cell parameters were obtained by least-squares refinement of 25 reflections ($25° \le 2\theta \le 30°$). The intensities of three standard reflections monitored, every 150 reflections, showed no appreciable decay during the data collection.

The crystal structure was solved by standard heavy-atom procedures. The positional and thermal parameters were refined by the block-diagonal-matrix least-squares method. The minimized function was $\sum w(|F_o| - |F_c|)^2$, where $w^{-1} = \sigma(|F_o|) + (0.015|F_o|)^2$. No attempt was made to locate hydrogen atoms in the structure analysis. Computational work was carried out by using standard programs in UNICS III[19] and ORTEP.[20] Crystallographic data are given in Table 1. Selected bond distances, angles, and dihedral angles are summarized in Tables 2−4. Listings of non-hydrogen atom coordinates and isotropic thermal parameters are given in Table S1. Anisotropic thermal parameters (Table S2) and full listings of bond distances (Table S3) and angles (Table S4) are also provided as Supporting Information.

(19) Sakurai, T.; Kobayashi, K. *Rikagaku Kenkyuusho Hokoku* (*Rep. Inst. Phys. Chem. Res.*) **1979**, *55*, 69.
(20) Jonson, C. K. *ORTEP II;* Report ORNL-5138; Oak Ridge National Laboratory: Oak Ridge, TN, 1976.

Table 3. Selected Bond Angles of **1** (deg)

N−Ru−N (trans)	173.9(2)−176.2(2)
N−Ru−N (cis)	89.7(2)−90.2(2)
C(CO)−Ru−N(Py)	175.0(2)
Ru−C(CO)−O(CO)	179.7(6)
C_α−N−C_α (av for OEP)	106.7(5)−108.2(5)
N−C_α−C_β (av for OEP)	108.2(6)−109.9(5)
N−C_α−C_m (av for OEP)	125.0(6)−126.4(5)
C_α−C_β−C_β (av for OEP)	106.3(5)−107.9(7)
C_β−C_m−C_β (av for OEP)	126.0(4)−126.6(7)
C_α−N−C_μ (av for H_2PyP_3P)	106.7(5)−107.9(5)
N−C_α−C_β (av for H_2PyP_3P)	108.7(6)−109.8(5)
N−C_α−C_m (av for H_2PyP_3P)	125.3(5)−126.6(5)
C_α−C_β−C_β (av for H_2PyP_3P)	105.5(5)−108.0(6)
C_β−C_m−C_β (av for H_2PyP_3P)	124.0(5)−126.6(5)

Table 4. Selected Dihedral Angles of **1** (deg)[a]

(OEP)p−(H_2PyP_3P)p	80.78(8)
(OEP)p−(Py)p	63.23(35)
(H_2PyP_3P)p−(Py)p	68.92(49)
(OEP)p−(N(Py)−C23)v	63.20(14)
(Py)p−(Ru−N(Py))v	160.48(18)
(OEP)p−(Ru−N(Py))v	82.72(10)

[a] p, plane; v, vector.

Electrochemical Measurements. Cyclic voltammetry and steady-state voltammetry were performed with a Fuso microelectrode potentiostat HECS 972 and a Fuso potential sweep unit HECS 321B. The data were recorded on a Graphtec WVX-2400 X-Y recorder or were digitized and stored in an NEC PC-9800 personal computer through a Riken Denshi TCDC-12-8000 transient recorder. Locally written software was employed for data collection and analysis. The working and the counter electrodes used in cyclic voltammetry measurements were a platinum disk electrode (i.d. = 1.6 mm) and a platinum wire, respectively. Cyclic voltammograms were recorded at a scan rate of 100 mV/s at 10 °C. The sample solutions in 0.1 M (TBA)PF_6-CH_2Cl_2 ((TBA)PF_6 = tetrabutylammonium hexafluorophosphate) were deoxygenated with a stream of argon. The reference electrode was Ag/0.01 M [$Ag(CH_3CN)_2$]PF_6, 0.1 M (TBA)PF_6 (acetonitrile), and the half-wave potential of the ferrocenium/ferrocene couple was +0.352 V. The working electrode used in steady state voltammetry measurements was a platinum microdisk electrode (i.d. = 30 μm). The counter and reference electrodes were the same as the cyclic voltammetry measurements. Steady-state voltammograms were recorded at a scan rate of 10 mV/s at 10 °C.

Other Measurements. ^{1}H NMR spectra were recorded on a JEOL-EX 270 spectrometer. IR spectra (KBr disk) were obtained with a Hitachi 270-50 infrared spectrophotometer. UV−vis spectra were recorded on a Shimadzu U best-30 or a Hitachi U-3410 spectrophotometer.

Results and Discussion

Crystal Structure of 1. The molecular geometry and labeling scheme of **1** is shown in Figure 2. For the sake of clarity, the ethyl substituents of the octaethylporphyrin core have been omitted. Crystallographic data are given in Table 1. Selected bond distances, angles, and dihedral angles are listed in Tables 2−4, respectively.

The crystal structure consists of two Ru(OEP)(CO)(H_2PyP_3P) molecules and two dichloromethane molecules in a unit cell. The bond distances of Ru−N(OEP) span the range 2.042(5)−2.066(5) Å (average 2.051 Å) as shown in Table 2. The average distance is almost the same as that of Ru(TPP)(CO)(EtOH) (2.049 Å)[21] and Ru(TPP)(CO)(Py) (2.052 Å).[22a] Other bond distances of the ruthenium porphyrin ring and axial porphyrin ring are similar to those of general porphyrin structures. The carbonyl ligand is coordinated to the ruthenium ion linearly with the 179.7(6)° angle of Ru−C(CO)−O(CO), which is similar to that of Ru(TPP)(CO)(Py).[22a] The bond length Ru−C(CO) of **1** (1.801 Å) is intermediate between those of Ru(TPP)(CO)(EtOH) (1.77 Å)[21] and Ru(TPP)(CO)(Py) (1.838 Å).[22a] The bond length Ru−N(Py) (2.237 Å) is longer than that of Ru(TPP)(CO)(Py) (2.193 Å).[22a] Some dihedral angles of **1**, illustrated and summarized in Figure 3 and Table 4, respectively, are also characteristic; i.e., the dihedral angle between the pyridyl ring and the octaethylporphyrin ring is 63.20° and the Ru−N(Py) bond is tilted by ca. 7.3° from the perpendicular to the octaethylporphyrin plane, though, in the corresponding

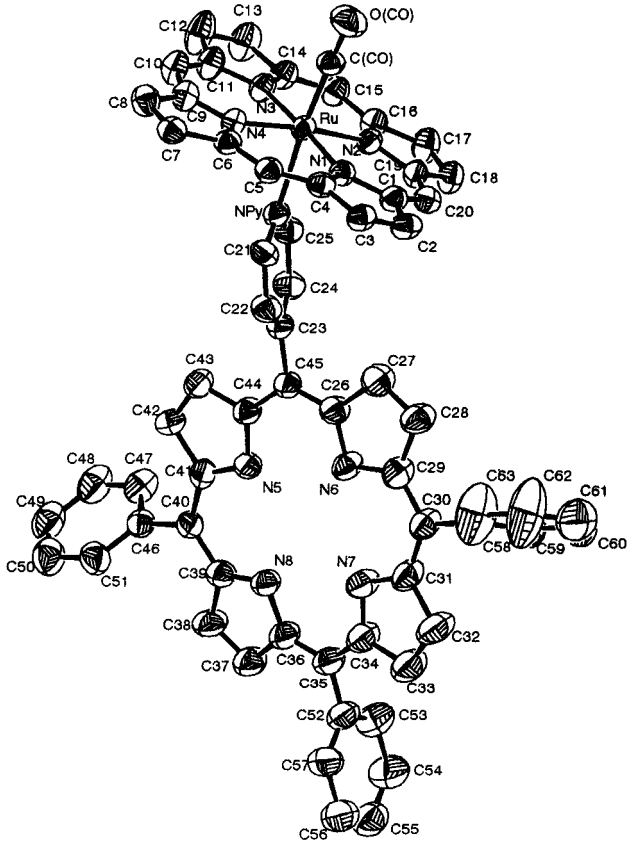

Figure 2. Molecular structure and atom labeling of Ru(OEP)(CO)(H_2PyP_3P) (**1**). Thermal ellipsoids are drawn to illustrate 50% probability surface.

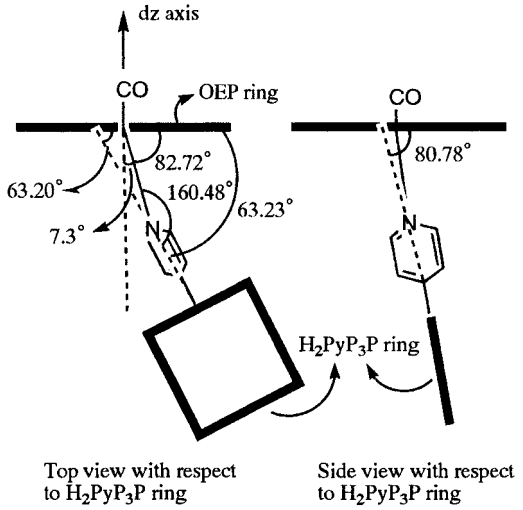

Figure 3. Brief illustrations of tilt and tipping angles to the axial porphyrin plane of **1**.

(21) Bonnet, J. J.; Eaton, S. S.; Eaton, G. R.; Holm, R. H.; Ibers, J. A. *J. Am. Chem. Soc.* **1973**, *95*, 2141.
(22) (a) Little, R. G.; Ibers, J. A. *J. Am. Chem. Soc.* **1973**, *95*, 8583. (b) Hopf, F. R.; O'Brien, T. P.; Scheidt, W. R.; Whitten, D. G. *J. Am. Chem. Soc.* **1975**, *97*, 277.

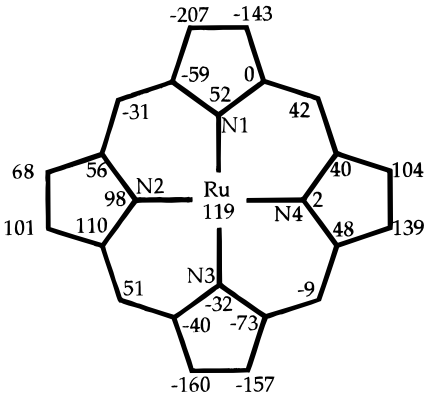

Figure 4. Diagram to illustrate the nonplanarity of the porphyrin skeleton of the ruthenium porphyrin ring. The numbers indicate the perpendicular displacement of an atom (in units of 0.001 Å) from the mean plane of the 24-atom core of the porphyrin. The Ru atom was not included in the plane calculation.

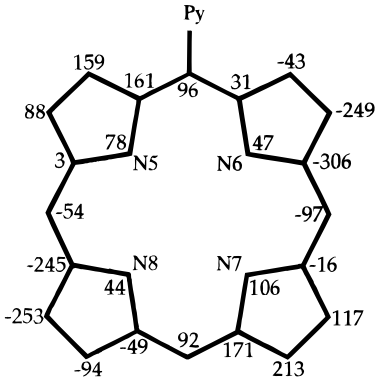

Figure 5. Diagram to illustrate the nonplanarity of the porphyrin skeleton of the axial porphyrin ring. The numbers indicate the perpendicular displacement of an atom (in units of 0.001 Å) from the mean plane of the 24-atom core of the porphyrin.

monomer complexes such as Ru(TPP)(CO)(Py)[22a] and Ru(OEP)-$(Py)_2$,[22b] the pyridyl rings and the ruthenium porphyrin rings are essentially perpendicular. The pyridyl ring is also tipped by ca. 19.5° (tipping angle: 160.48°) from the Ru−N(Py) bond toward the octaethyporphyrin plane. These features are characteristic of the porphyrin oligomers linked perpendicularly; i.e., the tilted and tipping angles for the Zn(PyP_3P) polymer were also observed to be 10 and 155.6(8)°, respectively.[8] This extensive tilt of bound pyridine of the Zn(PyP_3P) polymer was explained by the strain induced by polymerization besides crystal-packing effects.[8] However, we imagine that the tilt of the pyridyl ring of **1** is the result of crystal-packing effects as discussed later.

The ruthenium octaethylporphyrin macrocycle of **1** is not completely planar as shown in Figure 4. The ruthenium ion lies 0.119(1) Å out of the mean plane of the 24-atom core toward CO. This displacement is still larger than that of a monomeric analogue of Ru(TPP)(CO)(Py) with a corresponding value of 0.079 Å.[22a] The maximum displacement among the atoms of the ruthenium porphyrin macrocycle is 0.207 Å of C2 (β-pyrrole carbon), which is larger than that of Ru(TPP)(CO)(Py) by more than three times. The axial porphyrin macrocycle is also distorted significantly as shown in Figure 5. Displacements of several pyrrole carbon atoms from the mean plane of 24-atom core are more than 0.2 Å, which is also significantly larger than in free H_2TPP.[23]

The crystal of **1** has a layer structure of octaethylporphyrin rings as shown in Figure 6. The layer structure is composed of two kinds of layers; i.e., in the one layer, the ruthenium(II)

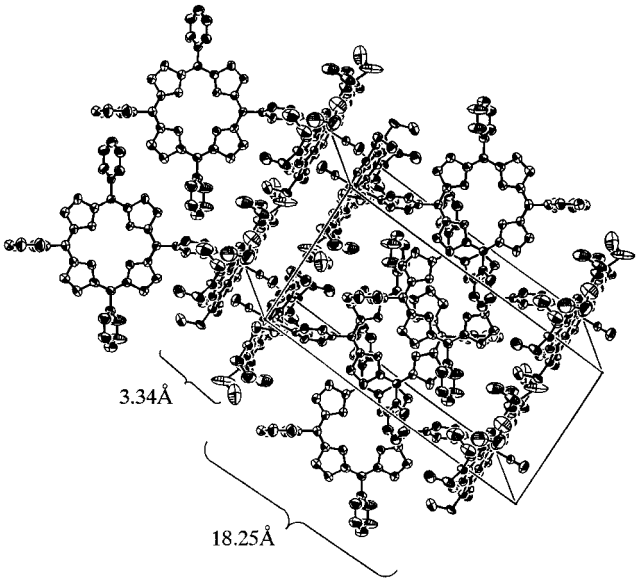

Figure 6. Packing description of **1**: Top view with respect to axial porphyrin macrocycles.

octaethylporphyrin subunits are aligned by interposing carbonyl ligands with a 3.34 Å layer distance. The octaethylporphryin macrocycles are not overlapping with each other. And in the other, the subunits are facing 18.25 Å apart, sandwiching the axial porphyrin ligands. The shortest distance between two carbons of the ethyl substituents of adjacent octaethylporphyrins is 3.899 Å. The axial porphyrin ligands are aligned horizontally. The axial porphyrin planes are superimposed alternately on adjacent axial porphyrin ligands. The mean-plane separation between the overlapped two porphyrin ligands is 4.24 Å. The shortest intermolecular atomic distances between the axial porphyrin ligands and between the axial porphyrin core atoms are found to be 3.726 Å for C37(β-pyrrole carbon)−C59(phenyl carbon) and 4.125 Å for N7−C34, respectively. In addition, the shortest distance between no overlapped adjacent axial porphyrins is 4.644 Å of C40−C42 and the mean-plane separation was 4.54 Å. Then, these mean-plane separations and shortest atomic distances between the adjacent axial porphyrin cores are too long to affirm the existence of $\pi-\pi$ interactions.[24,25] Hence, we think that the tilt of the pyridyl ring of **1**, discussed above, cannot be attributed to a strain between axial porphyrin subunits but mainly to crystal-packing effects.

^{1}H NMR Spectra. For the measurements of ^{1}H NMR spectra, carbonyl dimers and trimers **1**−**7** and bis(pyridyl) trimers **8**−**10** were dissolved in CD_2Cl_2 and C_6D_6, respectively.[26] All the Ru(II) porphyrin oligomers showed sharp ^{1}H NMR signals which indicated that these oligomers were all diamagnetic. The chemical shifts of the oligomers are listed in Table 5.

The spectrum of **1** revealed that the oligomer took on the dimeric structure even in solution. Integral intensities of the signals agreed well with the composition of 1:1 for OEP and

(23) (a) Silvers, S. J.; Tulinsky, A. *J. Am. Chem. Soc.* **1967**, *89*, 3331. (b) Chen, B. M. L.; Tulinsky, A. *J. Am. Chem. Soc.* **1972**, *94*, 4144. (c) Codding, P. W.; Tulinsky, A. *J. Am. Chem. Soc.* **1972**, *94*, 4151.
(24) (a) Hunter, C. A.; Sanders, J. K. M. *J. Am. Chem. Soc.* **1990**, *112*, 5525. (b) Blach, A. L.; Latos-Grazynski, L.; Noll, B. C.; Szterenberg, L.; Zovinka, E. P. *J. Am. Chem. Soc.* **1993**, *113*, 11846.
(25) Scheidt, W. R.; Lee, Y. J., *Struct. Bonding (Berlin)* **1987**, *64*, 1.
(26) Deuterated benzene C_6D_6 was used for the bis(pyridyl) complexes of **8**−**10** as a solvent, because the analogous complex of $Ru^{II}(OEP)(Py)_2$ was slowly oxidized in chloroform to generate the corresponding ruthenium(III) complexes which caused paramagnetic shifts and broadening in the NMR spectra.[22b]

Table 5. ^{1}H NMR Data for Ruthenium(II) Porphyrin Oligomers (CD_2Cl_2)

	axial ligand porphyrin subunit (H_2PyP_3P or *trans*-$H_2Py_2P_2$)				Ru porphyrin subunit (Ru(OEP), Ru(TPP), Ru(TTP))					phenyl (axial ligand or Ru(Por))	
ligand or complex	NH	2,6-Py	3,5-Py	β-pyrrole	*meso* (OEP)	CH_2 (OEP)	CH_3 (OEP)	β-pyrrole (TPP, TTP)	CH_3 (TTP)	*o*	*m,p*
H_2PyP_3P	−2.88	8.98	8.15	8.85						8.20	7.77
trans-$H_2Py_2P_2P$	−2.92	8.99	8.15	8.87						8.19	7.77
Ru(OEP)(CO)(ROH)[a]					9.95	4.11	1.94				
Ru(TPP)(CO)(ROH)[a]								8.67		8.25, 8.04	7.69
Ru(TTP)(CO)(ROH)[a]								8.69	2.66	8.07, 7.99	7.53
1	−3.41	1.23	5.77	8.69, 8.65, 8.36, 7.16	10.01	4.08	1.96			8.04, 7.95	7.68
1[b]	−2.90	1.82	5.20	8.76, 8.72, 8.18, 6.62	10.37	4.09	2.02			7.97, 7.85	7.45
2		1.26	5.79	8.78, 8.75, 8.45, 7.24	10.04	4.15	1.96			8.04, 7.94	7.67
3	−3.33	1.92	6.10	8.75, 8.70, 8.46, 7.30				8.75		8.32, 8.19, 8.08,8.00	7.7−7.5
4	−3.32	1.91	6.06	8.75, 8.72, 8.46, 7.30				8.75	2.67	8.19, 8.07, 8.01	7.7−7.5
5	−3.98	1.15	5.62	8.19, 7.01	9.97	4.03	1.90			7.7	7.7−7.5
6	−3.80	1.85	5.95	8.20, 7.19				8.69		8.29, 8.15, 7.97	7.7−7.4
7	−3.82	1.83	5.93	8.14, 7.17				8.71	2.65	8.15, 7.99, 7.80	7.8−7.5
8	−2.81	2.82	5.31	8.79, 8.77, 8.25, 6.93	10.06	4.09	2.08			8.01, 7.91	∼7.5
9		2.96	5.54	8.96, 8.92, 8.40, 7.11	10.10	4.11	2.07			∼8.11	∼7.5
10	−2.59	3.49	5.61	8.84, 8.82, 8.55, 7.55				9.01	2.46	8.48, 8.06, 7.95	∼7.5

[a] In $CDCl_3$. [b] In C_6D_6.

H_2PyP_3P porphyrins. The signals for the 2,6- and 3,5-protons of the pyridyl group of the axial porphyrin ligand were observed as doublets at the fields of 1.23 and 5.77 ppm, which were significantly higher than the corresponding resonance shifts of free H_2PyP_3P, at 8.98 and 8.15 ppm, respectively, as shown in Figure 7a. Similar upfield shifts have been observed for the pyridyl groups in an aggregated Zn(PyP_3P) polymer and in Ru(OEP)(CO)(Py).[8,27] The results clearly indicate the coordination of H_2PyP_3P to the central ruthenium ion of the Ru(OEP)(CO) core through the pyridyl group even in solution. The signals of β-pyrrole protons of the H_2PyP_3P part also indicate the coordination of this to Ru(OEP)(CO). The four signals observed at high-field regions at 7.16, 8.36, 8.65, and 8.69 ppm should be assigned to the protons located near the Ru(OEP)(CO) core as shown in Figure 7b. The chemical shifts of the OEP ring protons were not so different from those of Ru(OEP)(CO)(Py).[27] The inner NH proton signal was observed at −3.41 ppm.

Similar ^{1}H NMR results to **1**, i.e., upfield shifts of pyridyl protons, were also observed in the carbonyl dimers **2**−**4** except for the following. In the case of **2**, the absence of any signals around −3 ppm showed the substitution of the inner NH protons by a Zn(II) ion. The phenyl or tolyl proton signals of the ruthenium porphyrin rings of **3** or **4** could not be explicitly assigned, because of the overlapping of the signals with those of axial porphyrins. Nevertheless, the high-field shifts of the pyridyl and β-pyrrole protons of **3** and **4** indicated the formation of porphyrin dimers.

Table 6 shows the extent of upfield shifts ($\Delta\delta$) of 2,6- and 3,5-pyridyl protons of the porphyrin oligomers from the corresponding signals of the pyridyl group of free H_2PyP_3P. The respective $\Delta\delta$ values of −7.75 and −2.38 ppm for **1** in CD_2Cl_2 are very similar to those of Ru(OEP)(CO)(Py) (in $CDCl_3$). **3** also has comparable values. The similitude of $\Delta\delta$ values between the carbonyl dimers and the corresponding monomers and the sharpness of the pyridyl and four β-pyrrole proton signals indicate that the axial porphyrins are coordinated vertically to the Ru(II) ion with almost the same Ru−N(Py) distances as those of the corresponding monomers unlike the crystal structure of **1**. The $\Delta\delta$ values of **1** and Ru(OEP)(CO)(Py) are comparable even in C_6D_6. The $\Delta\delta$ values of **3** are smaller than those of **1**. The difference should mainly come from the difference in shielding effects of the ruthenium porphyrin rings.

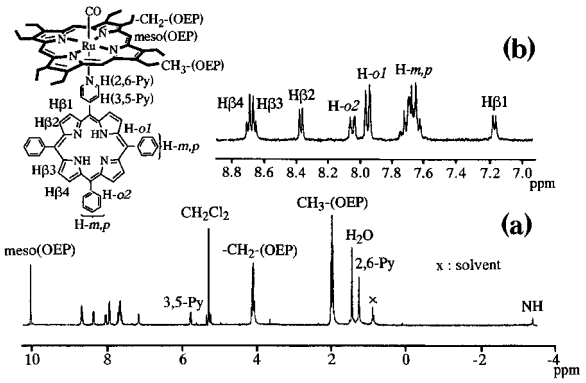

Figure 7. ^{1}H NMR spectrum of **1** in CD_2Cl_2: (a) In the region of −4 to 10 ppm; (b) in the region 7.0−8.8 ppm. The symbol "×" denotes solvent and solvent impurity peaks.

The signal intensities of the carbonyl trimers **5**−**7** revealed that the complexes consisted of two ruthenium porphyrin subunits and one bridging ligand of *trans*-$H_2Py_2P_2P$. Significant high-field shifts of the 2,6- and 3,5-pyridyl protons of *trans*-$H_2Py_2P_2P$ indicated that each trimer had a sandwich structure with a bridging *trans*-$H_2Py_2P_2P$. The resonances due to the protons of ruthenium porphyrin cores occurred around the magnetic fields similar to the corresponding carbonyl monomers of Ru(Por)(CO)(Py) and carbonyl dimers of **1**, **3**, and **4**. However, the two signals of the β-pyrrole protons of the bridging porphyrin ligands appeared at 7.0−7.2 and 8.2 ppm, though the carbonyl dimers showed four signals. The splitting patterns reflect each structure of these oligomers. In addition, the pyridyl protons and the inner NH protons appeared at higher fields than the dimers. The difference in chemical shifts of the inner NH proton resonances between the carbonyl trimers and the corresponding carbonyl dimers was ca. 0.5 ppm, and that between the carbonyl dimers and free H_2PyP_3P was again ca. 0.5 ppm. These results suggest that the ring currents of each ruthenium porphyrin in a molecule influence equally the inner NH protons located in the center of a bridging porphyrin ligand. Similar results were reported for [Ru(TPP)(CO)]$_4$($ZnPy_4P$)[11] and a series of osmium(II) porphryin oligomers.[12]

All ^{1}H NMR signals of the bis(pyridyl) trimers **8**−**10** in C_6D_6 were listed in Table 5. The signal intensities revealed that the complexes consisted of 1:2 fractions of ruthenium porphyrin

(27) Antipas, A.; Buchler, J. W.; Gouterman, M.; Smith, P. D. *J. Am. Chem. Soc.* **1978**, *100*, 3015.

Table 6. Chemical Shifts of Pyridyl Protons and Ruthenium Porphyrin Ring Protons and Chemical Shift Difference ($\Delta\delta$) from Free Pyridine (or H_2PyP_3P) or Corresponding Ruthenium Porphyrin Monomers[a]

compd	solv	2,6-Py	3,5-Py	4-Py	meso	$-CH_2-$	$-CH_3$
Ru(OEP)(CO)(Py)	$CDCl_3$	0.88 (−7.72)	4.89 (−2.31)	5.81 (−1.79)	9.79 (0)	3.97 (0)	1.89 (0)
	C_6D_6	1.26 (−7.30)	4.05 (−2.66)	4.56 (−2.47)	10.18 (0)	3.97 (0)	1.92 (0)
1	CD_2Cl_2	1.23 (−7.75)	5.77 (−2.38)		10.01 (0.22)	4.08 (0.11)	1.96 (0.07)
	C_6D_6	1.82 (−7.23)	5.20 (−2.76)		10.37 (0.19)	4.09 (0.12)	2.02 (0.10)
Ru(TPP)(CO)(Py)	$CDCl_3$	1.55 (−7.05)	5.21 (−1.99)	6.09			
3	CD_2Cl_2	1.92 (−7.06)	6.10 (−2.05)				
$Ru(OEP)(Py)_2$	C_6D_6	2.16 (−6.40)	4.08 (−2.63)	4.63 (−2.40)	9.65 (0)	3.88 (0)	1.92 (0)
8	C_6D_6	2.82 (−6.23)	5.31 (−2.64)		10.06 (0.41)	4.09 (0.21)	2.08 (0.14)
Py	$CDCl_3$	8.6 (0)	7.2 (0)	7.6			
Py	C_6D_6	8.56 (0)	6.71 (0)	7.03			
H_2PyP_3P	CD_2Cl_2	8.98 (0)	8.15 (0)				
H_2PyP_3P	C_6D_6	9.05 (0)	7.95 (0)				

[a] Values vs TMS. The values in parentheses show the chemical shift differences (− for the upfield shift) (2,6-Py, 3,5-Py) relative to free pyridine or H_2PyP_3P and the chemical shift differences (+ for the downfield shift) (*meso*, $-CH_2-$, $-CH_3$) relative to the corresponding ruthenium porphyrin monomers.

Table 7. UV−Vis Data for Ruthenium Porphyrin Oligomers

		λ_{max}/nm ($\epsilon/10^4$ M^{-1} cm^{-1})				
		Soret band		Q band	extra band	
complex	solv					
1	CH_2Cl_2	395 (30.4)	418 (40.1)	514 (3.16), 550 (2.98), 5.90 (0.54), 646 (0.40)		
2	CH_2Cl_2	395 (28.2)	419 (51.3)	516 (1.52), 548 (4.22), 586 (0.44)		
3	CH_2Cl_2		419 (69.0)	519 (2.75), 530 (sh), 550 (sh), 588 (0.61), 645 (0.40)		
4	CH_2Cl_2		417 (71.9)	519 (2.80), 530 (sh), 550 (sh), 589 (0.70), 647 (0.54)		
5	CH_2Cl_2	395 (51.3)	421 (38.7)	515 (4.69), 550 (6.30), 591 (0.53), 648 (0.37)		
6	CH_2Cl_2		414 (88.6)	520 (sh), 530 (4.51), 565 (sh), 589 (0.76), 646 (0.47)		
7	CH_2Cl_2		414 (92.0)	520 (sh), 532 (4.53), 565 (sh), 586 (0.81), 646 (0.47)		
8	$C_6H_5CH_3$	399 (sh)	419 (53.6)	516 (6.38), 546 (2.73), 588 (1.33), 652 (1.09)	456 (5.0)	650−750
9	$C_6H_5CH_3$	395 (17.1)	423 (66.7)	523 (4.07), 547 (4.57), 594 (0.91)	450 (sh)	653 (0.897)
10	$C_6H_5CH_3$		418 (67.2)	511 (5.87), 547 (1.81), 592 (1.47), 652 (1.36)		650−750
H_2PyP_3P	CH_2Cl_2		417 (44.9)	514 (2.0), 549 (0.78), 589 (0.61), 645 (0.40)		
Ru(OEP)(CO)(Py)[a]	CH_2Cl_2	396 (23.4)		518 (1.59), 549 (2.45)		
Ru(TPP)(CO)(Py)[b]	$CHCl_3$		413 (28.2)	495 (sh), 532 (1.78), 566 (0.37)		
$Ru(OEP)(Py)_2$[a]	C_6H_6	395 (10.2)		495 (1.48), 521 (3.80)	450 (1.58)	

[a] Reference 27. [b] Reference 21.

cores and axial porphyrin subunits. The axial porphyrin ligands also exhibited high-field shifts and the same splitting pattern with the corresponding carbonyl dimers, **1**, **2**, and **4**. These results apparently indicate that the complexes **8**−**10** are the trimers having two axial porphyrins. The ring current shifts of the pyridyl groups in **8** are comparable to those in Ru(OEP)-$(Py)_2$; i.e., the two axial porphyrins of **8** are coordinated perpendicularly to the ruthenium porphyrin core with the Ru−N(Py) distance similar to Ru−N(Py) in $Ru(OEP)(Py)_2$ in which the ruthenium ion is on the plane of the porphyrin ring.[22b]

The ring current of axial porphyrins in these oligomers caused only very slight downfield shifts on the resonances of ruthenium porphyrin ring protons. In comparison to the chemical shifts of the OEP ring protons of Ru(OEP)(CO)(Py), all shifts of the OEP rings of **1** were observed at lower field regions to a small extent. A maximal downfield shift was observed in the *meso*-protons which was the nearest to the axial porphyrins. The degree of the downfield shifts of **1** was not so sensitive to the difference in solvents such as CD_2Cl_2 and C_6D_6. Similar trends in the downfield shifts of OEP rings were observed in **8**, the magnitude of downfield shifts of **8** being nearly twice of **1**. Therefore, it is obvious that the extent of the downfield shift of OEP rings is proportional to the number of the axial porphyrins, suggesting that the sum of ring currents of two axial porphyrins determines the resonance shifts of protons of the ruthenium porphyrin ring.

As described above, comparable ring current shifts of pyridyl protons were observed between the carbonyl dimers (**1** and **3**) or the bis(pyridyl) trimer **8** and the corresponding ruthenium porphyrin monomers. This is in contrast to Zn porphyrin complexes. The $\Delta\delta$ values of the 2,6- and 3,5-pyridyl protons of the $Zn(PyP_3P)$ polymer, $Zn(TPP)(H_2PyP_3P)$, and Zn(TPP)-(Py) were reported as −6.4 and −1.9, −4.3 and −1.3, and −5.9 and −1.8 ppm, respectively.[8] The difference in the $\Delta\delta$ values between the $Zn(PyP_3P)$ polymer and Zn(TPP)(Py) was attributed to the change in tilt angle of the pyridine rings by the simulations of ring current effects. The estimated tilt angles of the $Zn(PyP_3P)$ polymer and Zn(TPP)(Py) were ca. 25 and ca. 0°, respectively. Although the tilt of pyridine ring of $Zn(PyP_3P)$ tetramer was actually demonstrated by X-ray crystallographic determination, the X-ray result cannot explain the large deviation of the $\Delta\delta$ values of $Zn(TPP)(H_2PyP_3P)$. Judging from the ^1H NMR data of the ruthenium porphyrin oligomers, it is supposed that the disagreement in the $\Delta\delta$ values of Zn porphyrin complexes is caused by the dissociation of axial ligands from these Zn porphyrin cores, which results in the difference in downfield shifts of the pyridyl proton signals.[28]

UV−Visible Spectra of Ruthenium Carbonyl Complexes. The data for the absorption spectra of the carbonyl complexes (**1**−**7**) in dichloromethane and for the complexes with no carbonyl ligands (**8**−**10**) in toluene are tabulated in Table 7. Absorption spectra of the ruthenium carbonyl complexes were essentially the sum of those of ruthenium porphyrin subunits and free H_2PyP_3P porphyrins. The complexes **1**, **2**, and **5** showed two Soret bands of constituent porphyrin subunits. The absorptions at 395 and around 420 nm were ascribed to the bands of ruthenium OEP subunits and axial or bridging

(28) Anderson, H. L.; Hunter, C. A.; Meah, M. N.; Sanders, J. K. M. *J. Am. Chem. Soc.* **1990**, *112*, 5780.

porphyrin ligands, respectively. There are no large changes in the wavelengths of the absorption bands from the bands of the parent compounds of Ru(OEP)(CO)(Py)[27] and free axial porphyrin ligands. Complex **5** in dichloromethane has absorption bands at 395 and 421 nm with higher intensity and a relatively small intensity, respectively, reflecting the formula composed from a 2:1 ratio for ruthenium porphyrin subunits and bridging porphyrin subunits. In fact, the molar absorptivity at 395 nm with 51.3×10^4 M^{-1} cm^{-1} is nearly equivalent to twice that of the molar absorptivity of Ru(OEP)(CO)(Py). In addition, the Soret absorption maximum of OEP part of **5** is not different from those of **1**, **2**, and Ru(OEP)(CO)(Py). These results are in sharp contrast to the fact that many porphyrin oligomers having face-to-face conformation show blue shifts of the Soret bands relative to the parent monomers.[3i,j,28,29] The absorption properties of these face-to-face porphyrin oligomers are understood as the excitonic interactions between the porphyrin rings, as described by the Kasha model;[1b,3d,30] i.e., the degree of a Soret blue shift depends on the distance between porphyrin rings.[1b,30] It may be that in the complex **5** the distance between the two ruthenium porphyrin cores is too large to allow interaction.

In the cases of complexes **3**, **4**, **6**, and **7** having ruthenium tetraarylporphyrin moieties, the Soret bands were observed as an apparent one intense band because of the similar Soret band energies between ruthenium porphyrin subunits and axial porphyrin subunits.[21] The molar absorptivity of the Soret band for each dimer and trimer complex is essentially equal to the sum of molar absorptivities of its components. In the Q band region from 515 to 565 nm, absorption spectra of all carbonyl complexes are also regarded as overlap of those of both core and ligand porphyrin subunits. The bands around 590 and 645 nm are essentially the absorptions of axial porphyrins.

UV−Visible Spectra of Ruthenium Bis(pyridyl) Complexes. Unlike carbonyl complexes, the ternary porphyrins, **8**−**10**, with no carbonyl ligands have extra bands besides the corresponding bands of the parent porphyrin subunits. For instance, the complexes **8** and **9** showed an intense extra band around 450 nm, which can be assigned to $d\pi(Ru^{II})-\pi^*(OEP)$ MLCT, similarly to $Ru(OEP)(Py)_2$.[27] The significant large molar absorptivity of the band of **8** (5×10^4 M^{-1} cm^{-1}) as compared with that of $Ru(OEP)(Py)_2$ (1.58×10^4 $M^{-1}cm^{-1}$) might raise some doubts about the assignment of the band. However, the following facts support the proposed assignment: The bands of the two complexes were decreased in intensity by the stoichiometric oxidation of Ru(II) to Ru(III) using $(NH_4)_2Ce(NO_3)_6$ as shown in Figure 8.[31] Furthermore, the band shifted remarkably to a longer wavelength in more polar solvents, while the bands originated from Ru(OEP) and H_2PyP_3P gave essentially no shifts. For example, the characteristic band of **8** shifted from 456 nm in toluene (dielectric constant: 2.4)[32] to 466 nm in tetrahydrofuran (7.4) and 475 nm in dichloromethane (8.9). The observed solvent effect is typical of the metal to ligand charge transfer band. Thus the bands should be assigned to MLCT from the ruthenium ion to the horizontal porphyrin ring.[33] The characteristic absorption band was also observed for the complex **9** around 450 nm but not observed for the TTP complex **10** as well as $Ru(TPP)(Py)_2$.[34]

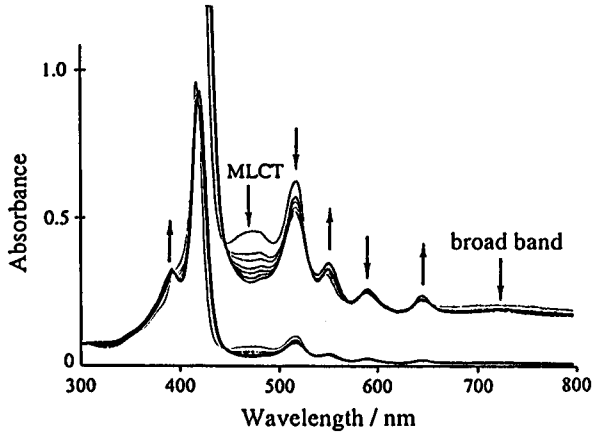

Figure 8. UV−vis spectral change of **8** (CH_2Cl_2 solution) by the addition of the CH_3CN solution of $(NH_4)_2Ce(NO_3)_6$.

Further, for **8**−**10**, one more extra broad band was observed in the region of 650−750 nm with molar absorptivities of about 8000 M^{-1} cm^{-1}. The band was also decreased in intensity by the stoichiometric oxidation of $Ru^{II}(OEP)(H_2PyP_3P)_2$ (**8**) with $(NH_4)_2Ce(NO_3)_6$ to form $[Ru^{III}(OEP)(H_2PyP_3P)_2]^+$ as shown in Figure 8. The peak maximum was at the wavelength around 675 nm for **9** and was at 725 nm for **8.** $Ru(OEP)(Py)_2$ exhibits very weak near-IR bands around ∼645 (sh) and ∼715 (sh) nm, which are assigned to forbidden CT $d-e_g(\pi^*)$ transitions.[27] The near-IR bands of **8**−**10** are too intense to assign to the forbidden CT transitions and are tentatively assigned to CT bands between two axial porphyrins via ruthenium(II) ions.

The Soret bands of three complexes are also not simple overlaps of the corresponding bands of the ruthenium porphyrin subunits and the axial porphyrin subunits. The complex **8** exhibits a broad Soret band with a peak maximum at 419 nm and a shoulder around 400 nm. The Soret band is seemingly composed of overlaps of those of the ruthenium porphyrin subunit (399 nm) and the axial porphyrin subunits (417 nm). However, the molar absorptivity at 419 nm (53.9×10^4 M^{-1} cm^{-1}) is much smaller than the expected value for two H_2PyP_3P (ca. 90×10^4 M^{-1} cm^{-1}). While the molar absorptivity of an axial porphyrin of the carbonyl complex **1** is smaller than that of the free H_2PyP_3P (ca. 45×10^4 M^{-1} cm^{-1}),[35] the extent of the decrease for **8** is much more. Furthermore, in the spectral change of **8** by the reaction with pyridine to generate $Ru^{II}(OEP)(Py)_2$ and two free H_2PyP_3P, the Soret band at 419 nm of axial porphyrins shifted to 417 nm and increased in intensity significantly. These characteristic features of the

(29) (a) Tran-Thi, T. H.; Lipskier, J. F.; Maillard, P.; Momenteau, M.; Lopez-Gastillo, J.-M.; Jay-Grein, J.-P. *J. Phys. Chem.* **1992**, *96*, 1073. (b) Hunter, C. A.; Meah, M. N.; Sanders, J. K. M. *J. Am. Chem. Soc.* **1990**, *112*, 5773.

(30) (a) Kasha, M.; Rawls, H. L.; El-Bayoumi, M. A. *Pure Appl. Chem.* **1965**, *11*, 371. (b) Kasha, M. *Radiat. Res.* **1963**, *20*, 55. (c) Hunter, C. A.; Sanders, J. K. M.; Stone, A. J. *Chem. Phys*. **1989**, *133*, 395.

(31) Metalloporphyrins can be oxidized either at the metal center or at the porphyrin rings to generate π-cation radicals. The bis(pyridyl) complex **8** can be oxidized at the three parts, i.e., the metal center, the ruthenium porphyrin ring, and the axial porphyrin rings. If a π-cation radical was generated, the absorption spectrum should cause a significant change, i.e., relative broad bands should appear in the region 500−700 nm and the Soret band should be broadened. However, no broad band was observed in the region in the oxidation process of **8**. In addition, the shoulder around 400 nm, which can be assigned to the Soret band of OEP, is blue-shifted. These spectral changes fitted well the change in the oxidation process of $Ru^{II}(OEP)(Py)_2$ to generate $[Ru^{III}(OEP)(Py)_2]^+$; i.e., the oxidations of **8** occurred at the metal center to form $[Ru^{III}(OEP)(H_2PyP_3P)_2]^+$ and π-cation radicals were not generated on either the metalloporphyrin ring or the axial porphyrin rings. This observation is consistent with the results of electrochemical studies described below in the text.

(32) Wollmann, H. *Pharmazie* **1974**, *29*, 708.

(33) Marvaud, V.; Launay, J. P. *Inorg. Chem.* **1993**, *32*, 1376.

(34) Brown, G. M.; Hopf, F. R.; Ferguson, J. A.; Meyer, T. J.; Whitten, D. G. *J. Am. Chem. Soc.* **1973**, *95*, 5939.

(35) The molar absorptivity of the axial porphyrin subunit of **1** is 43.9×10^4 M^{-1} cm^{-1} in toluene, which is larger than that in dichloromethane (40.1×10^4 M^{-1} cm^{-1}).

Scheme 1

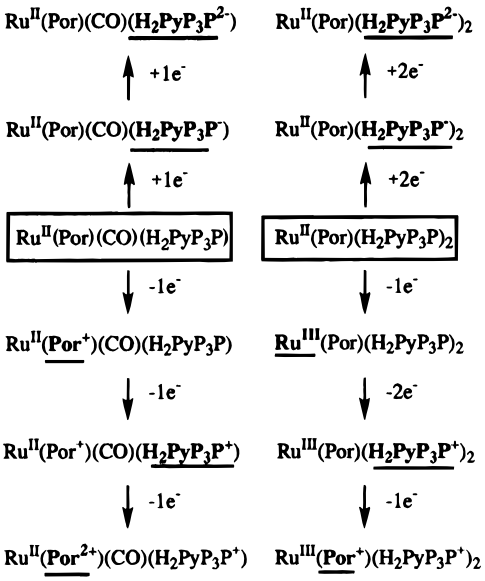

absorption spectra were also observed in the complexes **9** and **10**. Although the distinct split of the Soret bands, which was direct evidence of excitonic interaction as reported for various gable and flat porphyrin dimers linked covalently,[1b,i,3d,g,28,30,36] was not observed, those results clearly suggest the presence of excitonic interactions between two axial porphyrin ligands.

Electrochemical Studies. The electrochemical properties of ruthenium porphyrin oligomers in dichloromethane were studied by cyclic voltammetry and steady-state voltammetry. The results are schematically shown in Scheme 1, and the data are listed in Table 8.

The free porphyrin of H_2PyP_3P showed a reversible oxidation wave at 0.94 V and two reversible reduction waves at −1.30 and −1.63 V vs Ag/Ag^+ in 0.1 M $(TBA)PF_6-CH_2Cl_2$ solution as shown in Figure 9a. The corresponding three redox waves were also observed for H_2TPP. Thus, these redox processes should be ascribed to the formation of a monocation radical, a monoanion radical, and a dianion, respectively.[34,37] Beside these peaks, a small cathodic peak was observed around 0.6 V for the free H_2PyP_3P when scanned to 1.0 V. The peak became more distinct when scanned to 1.5 V. This redox behavior was not observed for H_2TPP. However, the H_2TPP solution containing nucleophilic pyridine or 4,4′-bipyridine exhibits a very similar redox profile with a cathodic peak around 0.6 V (vs SCE).[38] Under the conditions, the cathodic peak was ascribed to the chemical reaction to generate a β-substituted porphyrin after the oxidation of H_2TPP ring.[38] Therefore, certain chemical reactions such as dimerization or polymerization of H_2PyP_3P must also take place in the case of H_2PyP_3P, though the characterization of the products was not performed. In addition, the cathodic peak was not observed in the ruthenium porphyrin oligomer of **8** as shown in Figure 9d, because of the ligation of the pyridyl substituents to the ruthenium(II) ion.

The ruthenium carbonyl dimer of **1** exhibited a reversible one-electron oxidation wave at 0.53 V as shown in Figure 9b. The oxidation was assigned to the formation process of π-cation radicals on the ruthenium porphyrin ring, because the oxidation waves of $Ru(OEP^+)(CO)(L)/Ru(OEP)(CO)(L)$ (L = Py or

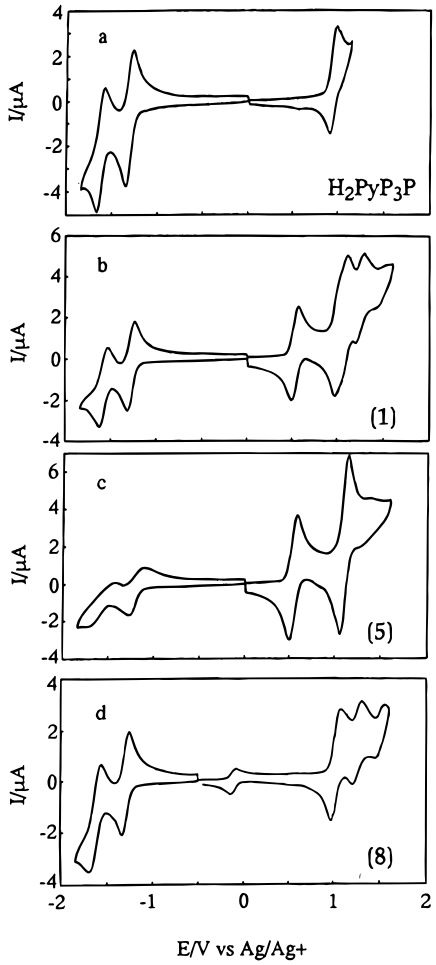

Figure 9. Cyclic voltammograms of H_2PyP_3P, **1**, **5**, and **8** in 0.1 M $(TBA)PF_6-CH_2Cl_2$ at 10 °C.

vacant site) couples were observed around 0.65−0.70 V (vs SCE).[34,39] Other carbonyl dimers, **3** and **4**, showed the oxidation waves of ruthenium porphyrin rings at 0.74 and 0.68 V, respectively. In the region higher than 1.0 V, the oxidation waves at 1.01 V were overlapped with the one at 1.09 V for **1** and around 1.20−1.25 V for **3** and **4**, respectively. The comparison of the heights of the overlapped waves to those of the first oxidation waves corresponding to the reversible one-electron oxidation of the ruthenium porphyrin ring revealed that the overlapped wave (>1.0 V) is an overall two-electron process. The former one in the two oxidation waves should be assigned to the first oxidation processes of an axial ligand porphyrin ring and the latter one the second oxidation processes of ruthenium porphyrin rings in comparison of redox profiles between **1**, **3**, and **4**. The ruthenium(II) porphyrin complexes having carbonyl ligands show no Ru(II) oxidation processes.[34,39] In carbonyl dimers (**1**, **3**, and **4**) and trimers (**5** and **7**), oxidation occurred at the porphyrin rings rather than the ruthenium center.

The dimers, **1**, **3**, and **4,** also exhibited two one-electron reduction waves in the potential region lower than −1.0 V, while the corresponding ruthenium(II) porphyrin monomer analogues showed no reduction waves.[34,39a,b] These waves were at the potentials close to the free H_2PyP_3P. Hence those waves can be assigned to the reduction of the axial ligand porphyrins. The redox potentials of axial ligand porphyrins slightly shifted to a

(36) (a) Won, Y.; Friesner, R. A.; Johnson, M. R.; Sessler, J. L. *Photosynth. Res.* **1989**, 201. (b) Anderson, H. L. *Inorg. Chem.* **1994**, *33*, 972.
(37) (a) Felton, R. H.; Linschitz, L. *J. Am. Chem. Soc.* **1966**, *88*, 113. (b) Heiling, G. P.; Wilson, G. S. *Anal. Chem.* **1971**, *43*, 545.
(38) Giraudeau, A.; Ruhlmann, L.; El Kahef, L.; Gross, M. *J. Am. Chem. Soc.* **1996**, *118*, 2969.
(39) (a) Felton, R. H. In *The Porphyrins*; Dolphin, D., Ed.; Academic Press: New York, 1979; Vol. 5, Chapter 3. (b) Brown, G. M.; Hopf, F. R.; Meyer, T. J.; Whitten, D. G. *J. Am. Chem. Soc.* **1975**, *97*, 5385. (c) Pacheco, G. M.; James, B. R.; Rettig, S. J. *Inorg. Chem.* **1995**, *34*, 3477.

Table 8. Electrochemical Data for Selected Porphyrin Oligomers[a]

complex	axial ligand (redn)		Ru(III/II)	$Ru(Por^+)/Ru(Por)$	axial ligand (oxdn)	$Ru(Por^{2+})/Ru(Por^+)$
H_2PyP_3P	−1.63 (56) [1]	−1.301 (57) [1]			0.943 (51) [1]	
$Ru(OEP)(CO)(H_2PyP_3P)$ (**1**)	−1.610 (57) [1]	−1.274 (60) [1]		0.532 (57) [1]	1.01 [1]	1.09 [1]
$Ru(TPP)(CO)(H_2PyP_3P)$ (**3**)	−1.600 (53) [1]	−1.263 (73) [1]		0.735 (56) [1]	1.012 (60) [1]	1.259 (48) [1]
$Ru(TTP)(CO)(H_2PyP_3P)$ (**4**)	−1.575 [1]	−1.268 (83) [1]		0.680 (51) [1]	1.010 (50) [1]	1.207 (52) [1]
$[Ru(OEP)(CO)]_2(H_2Py_2P_2P)$ (**5**)	−1.650 (88) [1]	−1.225 (84) [1]		0.538 (57) [1 × 2]	1.107 (58) [1][b]	1.107 (58) [1 × 2][b]
$[Ru(TTP)(CO)]_2(H_2Py_2P_2P)$ (**7**)	−1.587 [1]	−1.213 (76) [1]		0.701 (62) [1 × 2]	1.20 (81) [1][b]	1.20 (81) [1 × 2][b]
$Ru(OEP)(H_2PyP_3P)_2$ (**8**)	−1.658 (72) [1 × 2]	−1.292 (68) [1 × 2]	−0.114 (57) [1]	1.02 [1]	1.02 [1 × 2]	
$Ru(TTP)(H_2PyP_3P)_2$ (**10**)	−1.680 [1 × 2]	−1.281 (65) [1 × 2]	0.137 (63) [1]	1.125 (50[c]) [1]	1.03 (60)[c] [1 × 2]	

[a] Half-wave potentials ($E_{1/2}$) were obtained from the steady-state voltammograms with a platinum microelectrode. The numbers in parentheses are log-plot slope values in mV for the steady-state voltammograms. The numerals in brackets are the numbers of electrons transferred which are evaluated from the wave heights and the log-plot slopes. 1 × 2 means that two reversible one-electron processes occur at almost the same potential. [b] An overlapped wave. [c] Peak separation from CV.

positive direction as compared with those of free porphyrin ligands. This may result from the coordination of the axial porphyrin ligands at the site trans to the carbonyl ligands which have very strong π-acceptor properties.

The ruthenium carbonyl trimers, **5** and **7**, showed characteristic redox properties similar to the dimers of **1** and **4**. The two one-electron oxidation waves of two ruthenium porphyrin rings were observed at 0.54 V for **5** (Figure 9c) and 0.70 V for **7** as a perfectly overlapped reversible wave with the log plot slope of ca. 60 mV similar to those of dimers of **1** and **4**. These results indicated that the ruthenium porphyrin rings in a molecule were oxidized almost independently at the same potentials. In the potential region higher than 1 V, three-electron processes, composed of the first oxidation step of bridging porphyrins and the second oxidation step of two ruthenium porphyrin rings, were observed. Similarly, the two one-electron reduction waves of the bridging ligands, observed in the negative region lower than −1.0 V, appeared at potentials higher than those for **1** and **4**. This is because the two pyridyl substituents of the bridging porphyrins coordinate to the sites trans to carbonyl ligands.

In contrast to the ruthenium carbonyl complexes, the bis(pyridyl) trimers **8** and **10** afforded the characteristic one-electron oxidation waves of the Ru(III)/Ru(II) couples at −0.11 (Figure 9d) and 0.13 V, respectively. The different potentials reflect electron-donor abilities of the two different ruthenium porphyrin rings, similarly to the relation between $Ru(OEP)(Py)_2$ (0.08 V vs SCE) and $Ru(TPP)(Py)_2$ (0.21 V vs SCE).[34,39] Other anodic waves were also observed at 0.99 V for **8** and 1.05 V for **10**, though the electron number of these processes could not be exactly confirmed by steady-state voltammetry since presumably the complexes were adsorbed on the electrode as $[Ru^{III}(Por)(H_2PyP_3P)_2]PF_6$. The processes should be three-electron processes composed of the first oxidation of two axial porphyrin rings and the first oxidation of a ruthenium porphyrin ring, because all the three porphyrins species, H_2PyP_3P, $[Ru^{III}(OEP)(Py)_2]^+$, and $[Ru^{III}(TPP)(Py)_2]^+$, gave the first oxidation waves of porphyrin rings to generate π-cation radicals at the potentials around 0.8−1.0 V vs SCE.[34,39a]

Two reduction waves of the axial ligand porphyrins of **8** were observed at −1.29 and −1.66 V and those of **10** at −1.28 and −1.68 V as an overlapped two-electron process, respectively. The potential values are very similar to the values of free porphyrins. As no separation of the waves was observed, it is clear that two axial porphyrins were reduced independently at the same potential. In addition, these results suggest that the coordination of axial porphyrins through the pyridyl groups to ruthenium ions essentially causes no change in redox potentials on the axial porphyrin rings. Therefore, the positive shifts in redox potentials of the axial porphyrins in the carbonyl oligomers must be caused by the trans influence of carbonyl ligands.

Conclusion

Ruthenium(II) porphyrin dimers and trimers, **1**−**10**, with axial or bridging porphyrin ligands were synthesized and characterized by spectroscopic measurements.

The X-ray crystallographic structure analysis was performed on a carbonyl dimer of **1**. The axial porphyrin ligand is coordinated obliquely to the ruthenium porphyrin subunit through a pyridyl group. The ruthenium ion is displaced toward the CO ligand from the 24-atom mean plane by 0.119 Å. The ruthenium porphyrin plane and the axial porphyrin plane are significantly ruffled. An axial porphyrin macrocycle is facing another one in the neighboring molecule. The mean-plane separation of the porphyrin pair is 4.24 Å, which is still longer than that of $\pi - \pi$ interacting porphyrins.

^{1}H NMR spectra of **1** in solution reflected the dimer structure, i.e., the pyridine signals of the axial ligand porphyrin shifted to higher field dramatically by the shielding effect of the ruthenium porphyrin ring. The proton signals of the ruthenium porphyrin subunit were observed at chemical shifts similar to those of corresponding free monomer. The result confirmed that the coordination of the axial ligand porphyrin to the ruthenium porphyrin subunit through the pyridyl group was retained in solution. Other dimers and trimers, **2**−**10**, are also stable in solutions.

UV−visible spectra of the carbonyl dimers and trimers, **1**−**7**, were essentially composed of the spectra of the parent ruthenium porphyrins and axial or bridging porphyrins. The bis(pyridyl) trimers **8**−**10** suggested the presence of excitonic interactions between the two axial ligand porphyrins as revealed by the decrease in intensity accompanied by the broadening of the Soret bands. The complexes **8** and **9** exhibited characteristic MLCT bands around 450 nm.

Electrochemical analyses revealed that each porphyrin subunit comprising the porphyrin oligomers of **1**−**10** was reduced or oxidized separately; i.e., there is little interaction between the porphyrin subunits at least under the electrochemical conditions.

Acknowledgment. This work was supported by a Grant-in-aid for Scientific Research from the Ministry of Education, Science, and Culture of Japan (Nos. 08454206 and 06804034), by the 1994 Kawasaki Steel 21st Century Foundation, and in part by the 1993 Suhara Memorial Foundation.

Supporting Information Available: Tables of fractional coordinates and isotropic thermal parameters, anisotropic thermal parameters, bond lengths, and bond angles (Tables S1−S4) (9 pages). Ordering information is given on any current masthead page.

IC961154B